Design and Test of an Augmented Spark Igniter with Interchangeable Flow Control Orifices

Jacob J. Davies*, Cameron Harris†, Neer Patel‡, Ari Goldman§, and Dr. David Scarborough¶
Auburn University, Auburn, AL, 36839

Thomas W. Teasley‖
NASA Marshall Space Flight Center, Huntsville AL, 35812

An ultra-lean, modular augmented spark igniter was developed and validated for rocket engine test stand applications requiring extreme operational flexibility. The design employed interchangeable choked orifices to achieve independent control of the mass ratio and igniter chamber pressure while sharing gaseous oxygen and methane propellant supplies with the main chamber. Three experimental campaigns validated igniter performance: ten consecutive atmospheric discharge tests established repeatability, ten consecutive tests demonstrated fuel-rich main chamber ignition capability, and systematic variation from mass ratio 11.24 **to** 30.74 **and igniter chamber pressure** 627 **to** 2034 **kPa characterized operational limits. Combustion efficiency correlated strongly with chamber pressure (R^2 = 0.9371)**, **ranging from** 30% **at** 627 **kPa to** 95% **at** 2034 **kPa, with the relationship arising from propellant stay time effects quantified through characteristic chamber length. Higher pressure increases gas density and extends propellant stay time for fixed chamber geometry, enabling more complete combustion. The combustion efficiency and normalized characteristic length correlation (R^2 = 0.9647) provide insight into igniter performance and design guidance for specific pressure regimes. The plasma-assisted configuration with momentum controlled flame location enabled reliable ultra-lean operation while igniting fuel-rich main chamber propellants. A low-cost commercial off-the-shelf approach provided flexible ignition capability for subscale rocket engine testing requiring variable and extreme operating conditions across wide mass ratio and pressure ranges.**

I. Nomenclature

P	=	pressure
P_c	=	chamber pressure
P_0	=	stagnation pressure
T_0	=	stagnation temperature
γ	=	gas specific heat ratio
ρ	=	density
R	=	specific gas constant
u	=	velocity
Z	=	compressibility factor
MR	=	oxidizer to fuel mass ratio
$\dot{m}$	=	mass flow rate
C_d	=	discharge coefficient
D	=	diameter
$\bar{v}$	=	specific volume
τ	=	propellant stay time

*Graduate Student, Department of Aerospace Engineering, 141 Engineering Dr., AIAA Student Member
†Undergraduate Student, Department of Aerospace Engineering, 141 Engineering Dr., AIAA Student Member
‡Undergraduate Student, Department of Aerospace Engineering, 141 Engineering Dr., AIAA Student Member
§Graduate Student, Department of Aerospace Engineering, 141 Engineering Dr., AIAA Student Member
¶Associate Professor, Department of Aerospace Engineering, 141 Engineering Dr., AIAA Member
‖NASA Marshall Space Flight Center, Liquid Propulsion Systems Engineer, AIAA Member

C^* = characteristic velocity
L' = characteristic length
η = momentum flux ratio

II. Introduction

Rocket propulsion systems are a fundamental element of modern space exploration, satellite deployment, national defense capabilities, and the commercial spaceflight industry. As launch demand grows and mission profiles diversify, advanced propulsion concepts are being developed. These concepts promise higher performance, improved reliability, and reduced operational costs.

Novel rocket engine cycles, particularly rotating detonation rocket engines (RDRE), represent a significant departure from conventional designs. RDREs offer potential efficiency gains through pressure-gain combustion processes. However, these advanced concepts require extensive ground testing campaigns prior to flight qualification to validate theoretical predictions, characterize performance envelopes, and identify failure modes. The complexity and cost of these test campaigns make efficient and reliable test stand operations critical to propulsion development timelines.

Rocket engine test stands serve as proving grounds for theoretical designs. These facilities enable controlled experimentation under conditions that simulate flight environments. Test campaigns typically explore a wide parameter variation. Chamber pressure, mass ratios, and mass flow rates are often varied to characterize the aforementioned performance envelopes. Parametric exploration identifies optimal operating conditions, maps stability boundaries, and reveals unexpected phenomena that analytical models may not predict. Ground testing also validates computational fluid dynamics simulations, informs injector design iterations, and demonstrates hardware durability under thermal and mechanical loading. Propulsion development would require unacceptable risks in flight applications or prohibitively expensive development cycles without robust test infrastructure.

The ignition system represents one of the most critical subsystems in rocket engine testing. Test articles undergo numerous ignition cycles, unlike flight engines that may only ignite once per mission. Each ignition is expected to occur reliably, repeatedly, and safely, regardless of the main chamber operating conditions being tested. Igniters should be designed to reduce the chance of flashback that could damage the feed system or injector face. They must also avoid over-pressure transients that stress chamber walls. Ultimately, the test stand igniter should successfully initiate combustion across the parametric exploration of the test matrix. High combustion efficiency in the igniter ensures sufficient thermal energy delivery to the main chamber, particularly when igniting fuel-rich or oxygen-rich mixtures that fall outside conventional flammability limits [1, 2]. For test stands supporting novel engine concepts like RDREs, igniters may be required to accommodate extreme conditions. These extreme pressures, significant flow rate changes, and mass ratios far from stoichiometric conditions challenge conventional igniter designs.

Test stand igniters have evolved along different paths than flight engine igniters due to fundamentally different operational requirements. Flight igniters prioritize mass minimization, integration with flight propellant delivery systems, and qualification for the narrow operational envelope of a specific engine design [3]. Conversely, test stand igniters prioritize operational flexibility, durability during repeated cycling, and potentially compatibility with shared propellant infrastructure that serves multiple test articles. The test environment allows for heavier, more robust designs that would be impractical for flight but provide crucial advantages in development testing. Many test facilities have historically relied on external ignition sources, such as propane torches or pyrotechnic devices, to initiate combustion [4]. These approaches offer simplicity but introduce significant drawbacks. Propane systems may require separate fuel supplies and purge procedures. Pyrotechnic devices necessitate replacement between tests and generate debris that can disrupt instrumentation.

The test stand environment presents unique igniter requirements that differ fundamentally from flight applications. Limitations in external ignition sources become particularly challenging for test programs supporting advanced propulsion concepts like RDREs. Understanding conventional igniter architectures and their operational constraints provides essential context for addressing modern test stand requirements.

III. Background

Two primary categories of integrated test stand igniters have emerged: direct spark igniters (DSI) and augmented spark igniters (ASI) [5]. Direct spark igniters position electrodes directly in the main chamber propellant flow path. They then use a high-voltage discharge to ionize the chamber propellants to initiate combustion. The approach minimizes hardware complexity and eliminates the need for separate igniter propellant supplies. However, DSI systems suffer from

a limited operational range because they depend entirely on the conditions of the main chamber for ignition [6]. The spark must occur when the local mass ratio falls within flammability limits and flow velocities remain low enough to prevent flame blow-off [7]. Test campaigns exploring fuel-rich combustion for cooling studies or oxygen-rich conditions for efficiency characterization frequently push main chamber mixture ratios outside the DSI operational envelope. Electrode erosion and carbon fouling also become problematic during extended test campaigns. The erosion and fouling require frequent cleaning or replacement, which disrupts test schedules. The direct exposure to combustion products subjects insulators to thermal stress and chemical attack. The exposure can therefore lead to reliability concerns over numerous ignition cycles.

Augmented spark igniters address these limitations by incorporating a dedicated pre-combustion chamber where local conditions can be independently controlled relative to the main chamber [5]. The ASI receives propellant flows through separate supply lines, mixes them at optimal proportions near the spark source, and initiates combustion in a protected environment. Hot, reactive combustion products then discharge into the main chamber. The discharge provides thermal energy that promotes bulk propellant ignition even when the main chamber mixture ratios fall far outside conventional flammability limits. Igniter performance is decoupled from the main chamber operating conditions. Reliable ignition can then be achieved across the full parametric test matrix. The protected spark environment also reduces electrode erosion and fouling, extending maintenance intervals and improving campaign level reliability [8]. However, conventional ASI implementations for test stands typically require dedicated propellant supplies with independent pressure regulation and flow control. These additional components add to facility complexity, increase infrastructure costs, and create operational challenges when test campaigns require rapid turnaround between different propellant combinations or supply pressures.

Recent developments in plasma-assisted ASI configurations have demonstrated enhanced ignition reliability for hydrocarbon-oxygen systems through controlled oxidizer ionization [9]. These designs inject oxidizer flow around the spark-plug electrode, allowing the electrical discharge to ionize the oxygen molecules before they contact the fuel. The resulting plasma contains highly reactive species with significantly lower activation energy requirements than neutral molecules. When the ionized oxidizer subsequently encounters fuel injection, combustion initiates more readily and propagates more rapidly than conventional spark ignition. Deliberate control of the primary combustion location can be achieved through momentum flux ratio manipulation. By setting the oxidizer momentum flux higher than the fuel momentum flux, the flame front location can be biased toward the fuel inlet. The bias ensures complete oxidizer ionization before combustion begins. Biasing the flame front has been proven to be particularly effective for methane-oxygen propellants, where the relatively narrow flammability limits at atmospheric pressure can challenge conventional ignition approaches [7]. The plasma-assisted design also tolerates ultra-lean (high oxygen-rich) or ultra-rich (highly fuel-rich) pre-chamber operation, expanding the achievable operating envelope beyond traditional ASI design [9].

Despite these advances in test stand igniter technology, significant challenges remain for facilities conducting parametric testing of advanced propulsion concepts. Facilities can supply propellants from centralized systems for both igniters and test articles through shared pressure regulation and distribution networks. The centralized network eliminates the cost and complexity of a dedicated igniter propellant supply. However, the system constrains the igniter to operate using only the available supply pressures and propellant types without independent flow control. When test campaigns sweep through wide parameter spaces where main chamber pressure, mass ratio, and mass flow rates vary significantly, the shared supply system forces the igniter to accommodate these variations without active compensation. Cost-sensitive research environments favor designs using commercial off-the-shelf components rather than custom-machined parts. Crowded test article geometries can often demand compact packaging that fits within limited installation spaces. As mentioned before, igniters ought to be designed to prevent flashback, avoid over-pressure transients, and provide controlled ignition that minimizes thermal and mechanical shock to test hardware.

RDRE development programs intensify these challenges. RDREs operate at elevated pressures where conventional deflagrative igniters may struggle to deliver sufficient energy. Parametric studies exploring injector schemes, chamber geometries, and operating conditions require expansive test matrices [10]. Many test points fall far outside the igniter flammability limits where traditional spark igniters struggle to reliably function [11, 12]. The need for rapid test turnaround during iterative development campaigns demands igniters that resist thermal damage, electrode erosion, and carbon buildup across numerous ignition cycles. The combined requirements of a shared propellant supply system at these facilities, extreme parameter range, low cost, compact packaging, high durability, and reliable ignition across wide flammability limits present a significant design challenge.

Collaboration with NASA Marshall Space Flight Center (MSFC) for RDRE testing established additional design requirements that further constrained the igniter solution space. The igniter hot gas discharge path integrates through the

test article injector assembly, creating a risk of thermal damage to internal walls if flame temperatures exceed material limits. To mitigate the burn-through risk, the igniter must operate at ultra-lean (oxygen-rich) mass ratios that reduce combustion temperature while still providing sufficient energy for main chamber ignition. Simultaneously, the igniter must successfully initiate combustion in fuel-rich main chamber propellants typical of RDRE operation. DSIs lack the operational envelope to handle parametric testing across such wide mass ratio variations. Conventional ASIs provide operational flexibility but typically require dedicated propellant supplies with independent pressure regulation and flow control. The added complexity of the facility increases costs. External ignition sources, such as propane torches, avoid propellant system integration challenges but introduce safety risks and operational limitations that proved unacceptable during initial testing.

This work presents a solution through a modular ASI design that achieves independent control of mass ratio and chamber pressure using interchangeable choked orifices on a shared propellant supply. The study examined whether this approach could deliver reliable ignition across mixture ratios from 11 to 31 and chamber pressures from 600 to 2000 kPa while maintaining acceptable combustion efficiency. Three experimental test campaigns characterized igniter performance. The campaigns progressively validated repeatability, main chamber ignition capability, and operational envelope limits. The study quantifies the relationship between igniter chamber pressure and combustion efficiency to understand performance scaling and identify the physical mechanisms governing combustion losses.

Performance analysis revealed a strong linear correlation between chamber pressure and combustion efficiency ($R^2 = 0.9371$), while characteristic velocity efficiency (C^*_η) ranged from 30% at 627 kPa to 95% at 2034 kPa. C^*_η is the relative percentage of experimental to theoretical characteristic velocity under the given test conditions. The linear relationship suggests that combustion losses decrease substantially at elevated pressures, likely due to improved mixing timescales, enhanced chemical kinetics rates, or improved localized turbulence. Results from this work provide design guidance for test stand igniters supporting advanced propulsion development, demonstrate the viability of ultra-lean plasma-assisted ignition for methane-oxygen systems, and establish performance expectations for modular orifice-based flow control in shared propellant supply systems. The combination of ultra-lean igniter operation to protect hardware, an extreme parameter range, and low-cost commercial components presents a defined design challenge not addressed by existing literature.

IV. Methodology

A. Experimental Setup

The igniter was designed to meet the above requirements of low cost through commercial off-the-shelf components, high repeatability across numerous cycles, compact size for test article integration, and operational capability across wide mass ratio and chamber pressure ranges. The design was validated through three distinct test campaigns. The first two campaigns used identical igniter hardware configured for low-pressure operation. The first established igniter repeatability, and the second demonstrated main chamber ignition capability. A modification was made to the igniter hardware for the third campaign to achieve higher chamber pressures and explore extreme operating conditions.

The Auburn University Combustion Physics Laboratory operates a dual-propellant test facility with parallel oxygen and methane supply systems. Each propellant line began with a pressure regulator that set the supply pressure before each test. Once the supply pressures were set, the regulator maintained a constant pressure throughout the duration of the test. Braided stainless steel hoses connected the regulators to the test article. The hoses were 0.635 cm in diameter for oxygen and 1.27 cm for methane. The oxygen lines were sized to maintain flow velocities below 30.48 m/s. The size restriction helped to prevent impact ignition in the pure oxygen environment. The oxygen system was cleaned to CGA G-4.1 and ASTM G93 standards to eliminate the risk of particulate contamination. All tubing delivering propellants to the igniter was 1.27 cm in inner diameter.

Safety relief valves protected the system from overpressure by venting propellants away from the test article. The valves set the maximum system pressure at 2068.43 kPa and were sized to pass the full regulator flow rate at tank pressure (17926.37 kPa) in the event of regulator failure. Solenoid valves downstream of the relief connections provided remote flow control. Pressure transducers were installed immediately downstream of the solenoid valves to monitor supply conditions during testing. National Instruments CompactDAQ hardware acquired all sensor data. LabVIEW software was used to provide test sequencing, data logging, and safety interlock functions.

Figure 1 shows the complete test setup. The test article was mounted horizontally with the additively manufactured injector [10] positioned at the head end. The injector accepted three inputs: hot gas from the igniter (10), oxygen (2), and methane (3). The igniter was mounted directly to the injector through the hot gas path (4). Pressure transducers

(5) and (6) were installed upstream of each interchangeable metering orifice (7) and (8) to measure propellant supply conditions. An additional pressure transducer (1) measured the igniter chamber pressure in the cross fitting (9). The spark-plug (11) was threaded into the top port of the cross fitting. Orifice discharge coefficients were measured by flowing 689.47 kPa nitrogen gas through a calibrated Coriolis flow meter, recording upstream stagnation pressure, and applying the choked flow equation to calculate the effective flow area.

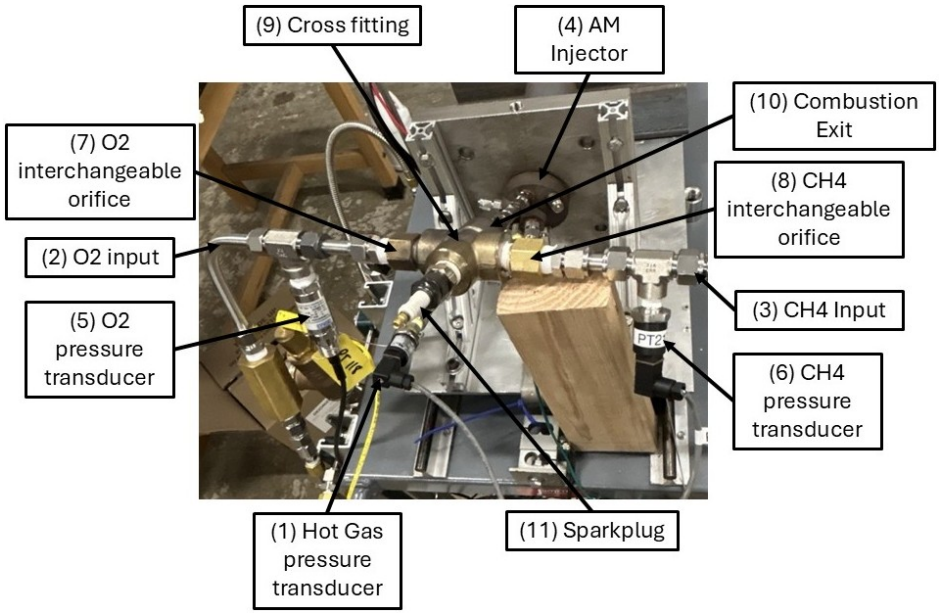

Fig. 1 Experimental test setup showing the low-pressure igniter configuration with oxygen (2) and methane (3) inputs, supply pressure transducers (5) and (6), hot gas pressure transducer (1), additively manufactured injector (4), cross fitting (9), interchangeable orifices (7) and (8), and spark-plug (11).

The igniter assembly consisted entirely of off-the-shelf components to minimize cost and enable rapid replacement. Figure 2 shows the cross-section of the design. A 304 stainless steel class 3000 NPT cross fitting (9) formed the main combustion chamber. A class 3000 rating was chosen to provide sufficient wall thickness for repeated oxygen-rich combustion exposure. The corrosive nature of hot oxygen at elevated pressure degrades thinner-walled fittings over numerous test cycles. The significant mass of the cross fitting also served as a heat sink, absorbing thermal energy during combustion and limiting external surface temperatures. Brass metering orifices (7) and (8) were threaded into 316 stainless steel NPT to tube fittings (13) that connected to the propellant supply lines. These orifices were readily interchangeable between tests, allowing systematic exploration of mass ratio and chamber pressure.

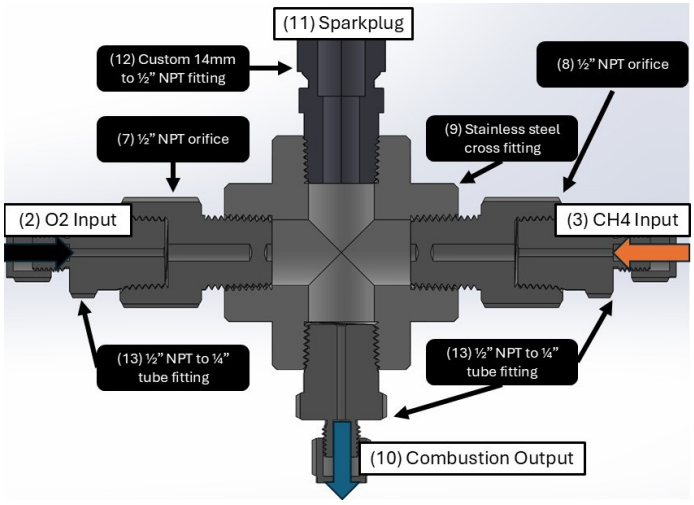

Fig. 2 Cross-sectional view of igniter assembly showing oxygen (2) and methane (3) inlets, combustion product exit (10), spark plug (11), metering orifices (7) and (8), 304 stainless steel cross fitting (9), custom M14 to 1.27 cm NPT adapter (12), and 1.27 cm NPT to 0.635 cm tube fittings (13).

MSFC requested the use of a spark-plug with M14 $\times$ 1.25 threading to match their test stand configuration. A custom 316 stainless steel adapter (12) was machined to convert to the cross fitting's 1.27 cm NPT threading. The spark-plug was positioned to be in the center of the cross fitting. For the low-pressure test campaigns, the initial electrode length of 3.81 cm was found to

over-penetrate into the combustion zone. The over-penetration resulted in the deepest 1.27 cm being incinerated due to prolonged exposure to the oxygen-rich flame. The electrode was then shortened to 2.54 cm and the top was positioned just inside the cross fitting volume without excessive thermal exposure. The shortened length provided reliable ignition for subsequent low-pressure testing.

The high-pressure campaign initially used a 0.1016 cm electrode to minimize flow blockage and thermal mass. However, the shorter electrode length failed to reliably ignite the propellant mixture. The spark plasma most likely dissipated before sufficient energy could be transferred to the surrounding gas. The 2.54 cm length from the low-pressure campaigns was then tested. The low-pressure length provided consistent ignition across the pressure range for the high-pressure campaign.

Two igniter hardware configurations were developed. The first was a low-pressure variant used in the first two test campaigns. The second was a high-pressure variant used in the third test campaign to further explore operational envelope characterization. The low-pressure variant used brass metering orifices that provided an adequate pressure rating and were off-the-shelf components. For the high-pressure variant, the brass orifices were replaced with 316 stainless steel orifices to accommodate increased supply pressures. The stainless steel orifices were laser drilled. An additional stainless steel orifice was placed at the exit of the high-pressure variant to simulate the minimum flow area of the actual test article hot gas path.

Oxygen and methane entered the cross fitting through opposing ports. Orifices were sized to maintain a greater oxygen momentum flux than methane momentum flux ($\eta > 1$), biasing the flame front location toward the fuel inlet. Once the spark-plug fired, the electrical discharge ionized the oxygen flowing past the electrode. The highly reactive oxygen then encountered the incoming methane flow, and the mixture ignited near the fuel inlet port. The resulting combustion products accelerated through the bottom port of the cross fitting and discharged to the injector. The momentum controlled ignition sequence ensured that oxygen ionization occurred before fuel contact to enhance ignition reliability and allow ultra-lean operation.

B. Orifice Sizing Determination

The orifice sizing process determines the required inlet orifice diameters that deliver the target igniter mass flow rate and mass ratio using the available supply pressures. The system was designed to achieve choked flow through both inlet orifices and the hot gas exit orifice. Choked conditions enabled independent control of igniter operating conditions despite sharing propellant supplies with the main test article. The sizing process began with determining the exit conditions. The exit conditions for the test campaigns were either atmospheric conditions or a main chamber.

The main chamber operated with gaseous methane and oxygen propellants. NASA Chemical Equilibrium with Applications (CEA) was used to determine the expected combustion product properties. These properties included temperature, specific heat ratio, molecular weight, and density. The solver was configured to use the "rocket" problem with equilibrium chemistry assumptions. A representative case from the first test campaign is shown using the following test conditions: chamber pressure of 1426.11 kPa, gaseous methane fuel at 294.26 K inlet temperature, gaseous oxygen oxidizer at 294.26 K inlet temperature, O/F ratio of 7.5, and expansion pressure ratio (P_c/P_e) of 2.0. The CEA solution provided the previously mentioned combustion product properties.

The igniter discharged hot combustion products through an exit orifice into the main chamber. Choked flow at this orifice was maintained by ensuring that the igniter chamber pressure exceeded the main chamber pressure by a sufficient margin. For choked flow through an orifice, the downstream pressure must be less than the critical pressure ratio. Therefore, the target igniter chamber pressure was set by ensuring the critical pressure ratio was achieved and thus guaranteeing choked exit conditions.

The maximum igniter temperature was limited by material compatibility and thermal damage concerns. The steel cross fitting that formed the igniter combustion chamber can withstand temperatures up to approximately 1200 K for short durations without losing structural integrity. Additionally, the MSFC requirement to prevent burn-through of internal test article walls constrained the hot gas temperature. Burn-through was addressed by operating the igniter at ultra-lean (oxygen-rich) mixture ratios. These mixture ratios reduce combustion temperature while maintaining sufficient energy for main chamber ignition.

With the target igniter chamber pressure and mass ratio set, compressible choked flow relations were then used to calculate the inlet orifice areas. Equation 1 relates the mass flow rate through a choked orifice to the upstream stagnation conditions:

$$\dot{m}_{igniter} = \frac{AC_d P_{0_{igniter}}}{\sqrt{T_{0_{igniter}}}} \sqrt{\frac{\gamma}{R}} \times \left(\frac{\gamma+1}{2}\right)^{-\left(\frac{\gamma+1}{2(\gamma-1)}\right)} \tag{1}$$

The compressibility factor (Z) was neglected for combustion products in Equation 1 as it reasonably approached unity under the conditions of interest. The mass flow rates for the oxidizer and fuel inlets were computed once the igniter exit orifice mass flow rate was determined from Equation 1. Equation 2 calculated the required oxygen mass flow rate:

$$\dot{m}_{O_2} = \dot{m}_{igniter} \times \frac{MR}{MR+1} \tag{2}$$

Similarly, Equation 3 determined the methane mass flow rate:

$$\dot{m}_{CH_4} = \dot{m}_{igniter} \times \frac{1}{MR+1} \tag{3}$$

REFPROP was used to obtain thermophysical properties for gaseous oxygen and methane under supply conditions (ambient temperature and specified supply pressures). Velocity using Equation 4 was computed for each propellant:

$$u = \sqrt{\gamma RT} \tag{4}$$

Equation 1 was rearranged to solve for the required orifice area, incorporating the added compressibility factor for each supply gas condition. Equation 5 expresses this relationship:

$$A_{orifice} = \frac{\dot{m}_{supply}\sqrt{T_{0_{ambient}}}}{C_d P_{0_{supply}} \sqrt{\frac{\gamma}{ZR}} \times \left(\frac{\gamma+1}{2}\right)^{-\left(\frac{\gamma+1}{2(\gamma-1)}\right)}} \tag{5}$$

Discharge coefficients (C_d) for each orifice were measured by flowing nitrogen through a calibrated Coriolis flow meter, measuring upstream stagnation pressure, and applying Equation 1 to calculate the effective flow area. The calibration process accounted for real orifice behavior, including boundary layer effects and geometric imperfections.

The plasma-assisted igniter design required oxygen ionization before fuel contact. Ionization was verified by calculating the momentum flux ratio between the oxygen and methane supply flows. Setting the oxygen momentum flux greater than the methane momentum flux biased the flame front location toward the fuel inlet. The bias ensured that the spark plasmas ionized oxygen before it reached the fuel. The momentum flux ratio (η) was calculated for each design condition using Equation 6:

$$\eta = \frac{\rho_{O_2} u_{O_2}^2}{\rho_{CH_4} u_{CH_4}^2} \tag{6}$$

All test configurations were designed to achieve $\eta > 1$. The intention was to use the momentum flux bias to position the primary igniter combustion zone closer to the fuel inlet.

Tables 1 and 2 illustrate the sizing methodology using representative conditions from early testing. Supply pressures and temperatures reflect actual facility capabilities. The mass ratio and orifice diameters shown correspond to the initial design calculation ($MR = 7.22$) for demonstration purposes. To characterize the igniter's operational envelope, we subsequently interchanged orifices spanning mixture ratios from 11.14 to 30.74, with complete test results presented in Table 3 in Appendix VII.

Combustion efficiency was evaluated for each test using characteristic velocity efficiency (C_η^*), which compares measured performance to theoretical predictions. A CEA analysis was performed for each test condition using the deflagration combustion equilibrium assumption to determine the theoretical characteristic velocity (C^*). Experimental characteristic velocity was calculated from the measured chamber pressure (P_c), exit area (A), and total mass flow rate ($\dot{m}_{total}$) using Equation 7:

$$C^* = \frac{P_c A}{\dot{m}_{total}} \tag{7}$$

Characteristic velocity efficiency (C_η^*), defined in Equation 8, quantifies how closely the igniter approaches ideal combustion performance:

$$C^*_\eta = \frac{C^*_{experimental}}{C^*_{theoretical}} \tag{8}$$

Values approaching 100% indicate near-complete combustion with minimal losses. Deviations from 100% reflect incomplete combustion, heat transfer losses, and non-equilibrium chemistry effects. C^*_η provided a standard basis for comparing igniter performance across different operating conditions and enabled correlation analysis between chamber pressure and combustion efficiency.

P_{O_2}	655	KPa
T_{O_2}	294.26	K
R_{O_2}	259.87	$\frac{m^2}{s^2 \times K}$
γ_{O_2}	1.40	
P_{CH_4}	379.21	KPa
T_{CH_4}	294.26	K
R_{CH_4}	518.23	$\frac{m^2}{s^2 \times K}$
γ_{CH_4}	1.32	
η	1.832	

Table 1 Supply conditions and thermophysical properties for representative igniter design: supply pressure (P), temperature (T), gas constant (R), specific heat ratio (γ), and momentum flux ratio (η).

$\dot{m}_{O_2}$	8.165×10^{-4}	kg/s
u_{O_2}	327.20	m/s
ρ_{O_2}	2.61	kg/m^2
$\dot{m}_{CH_4}$	9.07×10^{-5}	kg/s
u_{CH_4}	448.06	m/s
ρ_{CH_4}	0.758	kg/m^2
D_{O_2}	1.194	mm
D_{CH_4}	0.737	mm
MR	7.22	

Table 2 Calculated flow conditions and orifice dimensions: mass flow rate ($\dot{m}$), acoustic velocity (u), density (ρ), orifice diameter (D), and resulting mass ratio (MR).

V. Results and Discussion

Three test campaigns were conducted to systematically validate the igniter design and characterize its operational envelope. The first campaign established ignition repeatability by demonstrating ten consecutive successful ignitions with hot gas discharged into the atmosphere. The second campaign verified main chamber ignition capability by successfully igniting a fuel-rich main chamber through ten consecutive tests. The third campaign explored the igniter's operational limits by systematically varying mass ratio from 11.14 to 30.74 and igniter chamber pressure from 627 to 2034 kPa. The first two campaigns used identical igniter hardware, while the third required modified components to achieve chamber pressures exceeding 2000 kPa.

The first campaign demonstrated basic igniter functionality and established operational repeatability. Ten consecutive ignition tests were conducted under similar conditions to those listed in Tables 1 and 2. Hot gas was discharged directly to the atmosphere. All ten tests achieved successful ignition without hardware failure or performance degradation, which validated the mechanical design and established baseline operating characteristics.

Figure 3 is a time history of one test from this campaign. Methane flow was initiated at 1 second, and spark-plug discharge began simultaneously. Ignition occurred at 10 seconds when the oxygen supply reached the target pressure (551.58 kPa). Methane supply stabilized at 275.79 kPa. Both supply pressures remained constant throughout the 102 second test duration. The igniter maintained a steady mass ratio of 7.65 while the chamber temperature increased asymptotically. The chamber temperature reached approximately 1047 K at test completion. Spark-plug discharge was terminated once stable combustion was established at 10 seconds. The test concluded at 102 seconds with the simultaneous closure of both propellant valves.

The second campaign demonstrated the igniter's primary function: reliable initiation of combustion in a separate main chamber. The igniter was integrated with an additively manufactured single-element injector [10] that shared the common propellant supply. Unlike the first campaign, where hot gas vented to the atmosphere, these tests routed combustion products through an internal passage in the injector body into the main chamber. The main chamber operated fuel-rich at a mass ratio 1.3, representative of RDRE operating conditions. Ten tests were conducted with ten successful main chamber ignitions, demonstrating reliable performance with igniting off-stoichiometric propellant mixtures.

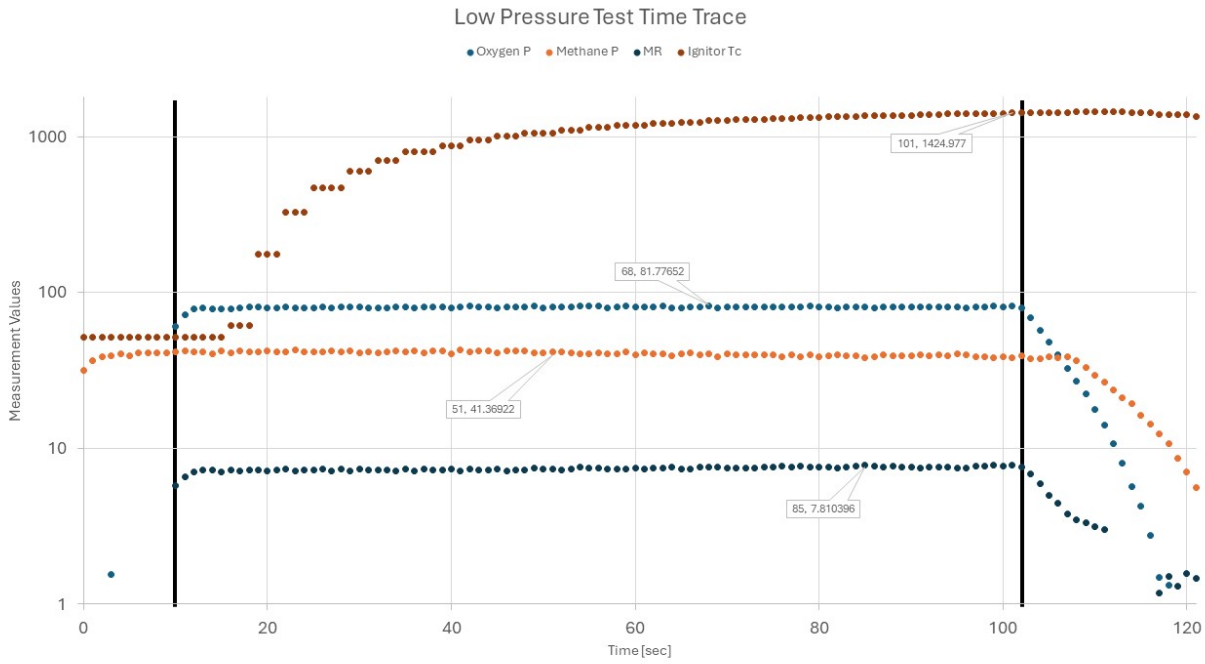

Fig. 3 Time history from low-pressure repeatability test showing oxygen pressure (blue), methane pressure (orange), mass ratio (gray), and igniter temperature (brown) on a logarithmic scale. Vertical black lines denote ignition (left) and shutdown (right). Supply pressures stabilized at target values while temperatures asymptotically approached steady state during the 102 second test.

Post-test inspection revealed thermal damage patterns that validated the momentum controlled ignition mechanism. Figure 4 shows the cross fitting after the test campaign. Surface charring concentrated on the methane inlet side (3) rather than being symmetrically distributed. The asymmetric patterns suggested that combustion occurred preferentially near the fuel inlet, as designed. The 304 stainless steel cross fitting withstood this repeated long-duration thermal exposure without noticeable structural damage, confirming adequate heat sink capacity.

The third campaign systematically explored the igniter's operational limits across extreme conditions. The hot gas exit returned to atmospheric discharge as in the first campaign, but the igniter hardware was modified to achieve higher chamber pressures. Specifically, a 0.16 cm diameter backpressure orifice was added at the hot gas exit to simulate an integrated main chamber hot gas path. Additionally, the brass metering orifices were replaced with laser drilled stainless steel orifices to accommodate higher supply pressures. The campaign objectives were to demonstrate self-ignition at mass ratios exceeding 25 and igniter chamber pressures above 2000 kPa. Both objectives were achieved with successful ignition at mass ratios up to 30.74 and igniter chamber pressures up to 2034

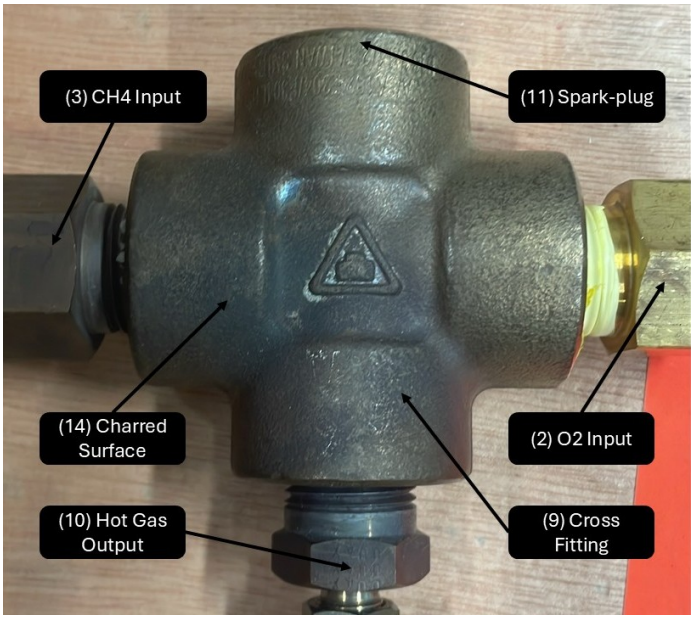

Fig. 4 Post-test condition of the igniter cross fitting (9) showing asymmetric thermal damage. Charring (14) concentrated near the methane inlet (3) rather than the oxygen inlet (2), suggesting momentum biased flame location. The cross fitting (9)retained structural integrity despite repeated oxygen-rich combustion exposure.

kPa. Table 3 in Appendix VII documents supply pressures, mass ratios, and igniter chamber pressures for all successful tests.

Figure 5 presents the characteristic velocity efficiency as a function of igniter chamber pressure for all successful tests in the third campaign. Combustion efficiency ranged from 30% at 627 kPa to 95% at 2034 kPa, exhibiting a strong linear correlation with igniter chamber pressure ($R^2 = 0.9371$). The linear correlation holds across the full mass ratio range tested (11.14 to 30.74), indicating that pressure, not mass ratio, dominates combustion efficiency. The linear trend suggests a fundamental physical mechanism linking pressure to combustion completeness.

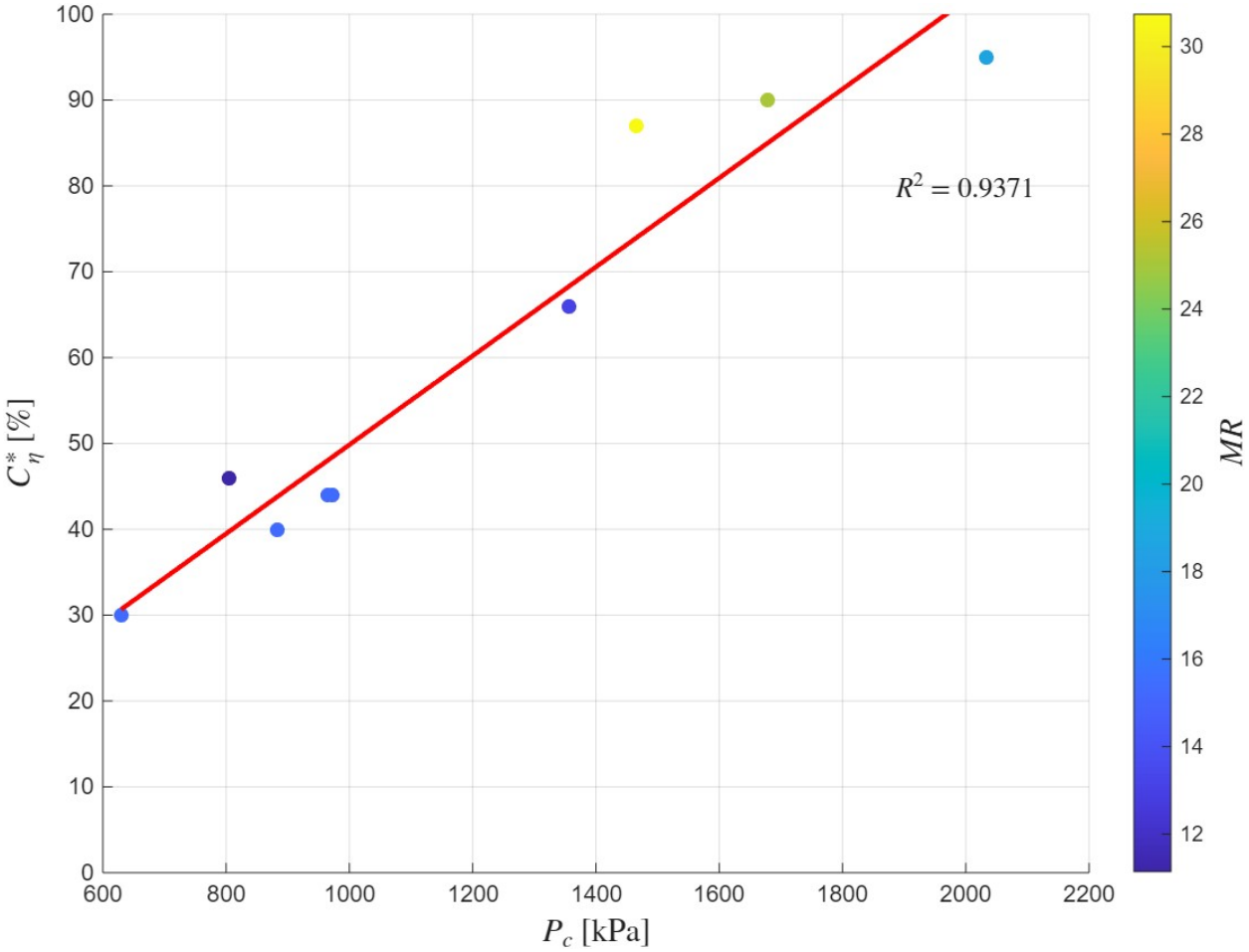

Fig. 5 Characteristic velocity efficiency versus igniter chamber pressure for all successful tests in the third test campaign. Marker color indicates mass ratio (colorbar). Linear regression (red line) shows strong correlation ($R^2 = 0.9371$) between pressure and efficiency. Performance improves consistently with pressure across full mass ratio range.

The strong pressure-efficiency correlation most likely arises from propellant stay time effects. Propellant stay time effects are quantified through the characteristic igniter chamber length (L'). Propellant stay time is the duration that reactions spend in the chamber before exiting [4]. Experimental L' was calculated using the relationship from Huzel and Huang [4]:

$$L' = \frac{\dot{m}\bar{v}\tau}{A_t} \tag{9}$$

where $\dot{m}$ is the calculated total mass flow rate, $\bar{v}$ is the average specific volume from CEA analysis, τ is the propellant stay time, and A_t is the throat (exit) area. The stay time was determined from the Reynolds number correlation developed by Tinker [5] for torch igniters. The correlation relates stay time to flow conditions through chamber geometry and fluid

properties. Tinker [5] showed that increasing the Reynolds number decreases the propellant stay time. Density is the driving factor in the change of Reynolds number for the igniter. Therefore, the Reynolds number relationship suggests that increasing density decreases propellant stay time.

Huzel and Huang [13] note that the effective L' for gas generators is roughly double that of a comparable main rocket engine. Due to extreme mass ratios, the igniter can be approximated as a gas generator. Normalized characteristic length, L'_η, was calculated by dividing the measured L' by twice the experimental length:

$$L'_\eta = \frac{L'_{actual}}{2 \times L'_{experimental}} \tag{10}$$

Figure 6 plots the igniter chamber pressure against the normalized characteristic length for the tests in the third campaign. A strong linear relationship ($R^2 = 0.8458$) was computed from regression. The linear correlation suggests that both $L'_{experimental}$ and L'_η are dependent on P_c. Figure 7 is then the next step and shows C^*_η plotted against L'_η. A highly linear relationship ($R^2 = 0.9647$) is noted. The relationship reveals the likely underlying mechanism outlined above: tests where experimental L' approached the physical L' achieved the highest efficiency because propellants remained in the chamber long enough for more complete combustion.

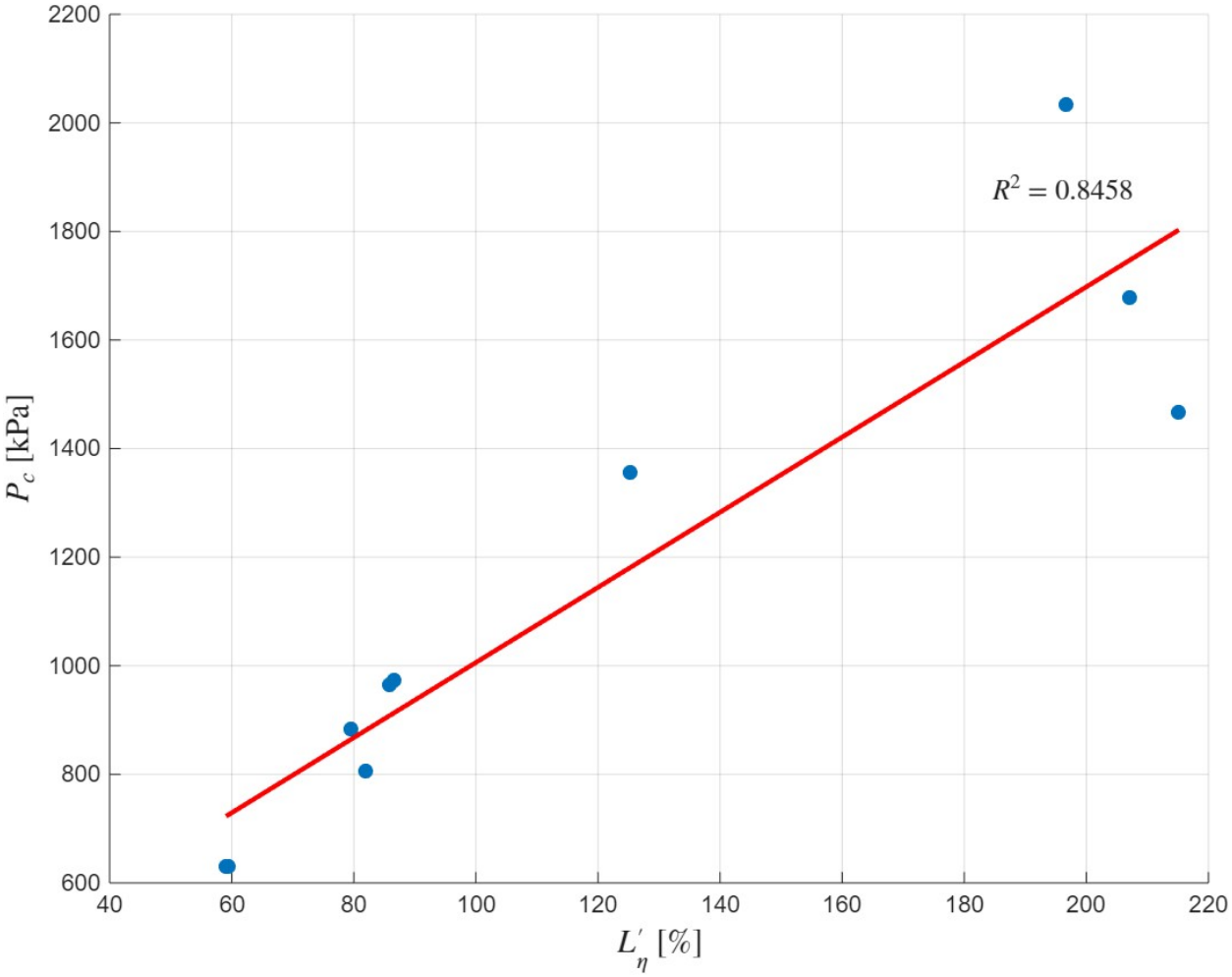

Fig. 6 Igniter chamber pressure versus normalized characteristic length for the third campaign. A linear fit (red, $R^2 = 0.8458$) shows pressure increased with increasing L'_η beyond physical chamber dimensions.

The characteristic length framework unifies the observed trends. Pressure affects efficiency not through a direct thermodynamic mechanism, but by increasing density and thus extending the propellant stay time for a given chamber

geometry. The linear C_η^* versus L'_η relationship (Figure 7) indicates that combustion completeness scales predictably with propellant stay time across the operating range. The linear C_η^* versus P_c relationship (Figure 5) then follows naturally because pressure determines density, which sets propellant stay time for fixed geometry. Chemical kinetics timescales decrease with pressure as reaction rates scale with density squared [14, 15], but the propellant stay time effects dominate the efficiency variation across the test conditions. Heat transfer losses become relatively less significant at higher pressure because combustion energy release scales with density, while wall heat flux increases only modestly [3].

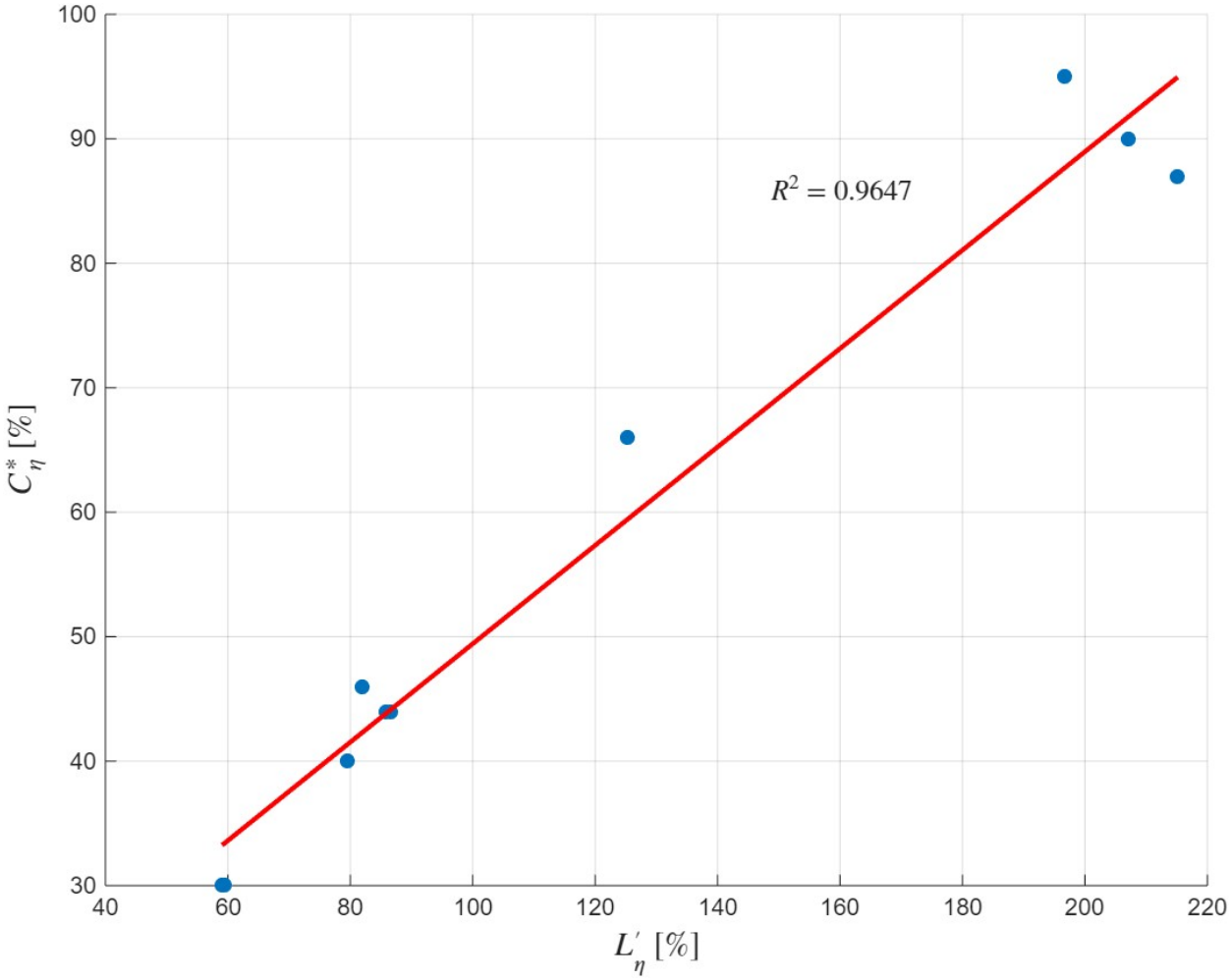

Fig. 7 Characteristic velocity efficiency versus normalized characteristic length for the third campaign. A linear fit (red, $R^2 = 0.9647$) shows efficiency increased with increasing L'_η beyond physical chamber dimensions. Tests operating above design L' achieved highest efficiency but also operated with the highest pressure.

The data reveal an important design trade-off. Tests operating well below the physical characteristic length achieve poor combustion efficiency because gases exit before combustion is complete. The igniter chamber is effectively too small for the operating pressure. Conversely, tests above the physical L' approach 90 to 95% combustion efficiency because the propellant stay time exceeds the chemical kinetics timescale [14, 15]. The cross fitting chamber volume provides adequate propellant stay time only at higher pressures where density is sufficient. The relationship suggests that for lower pressure operation, a larger chamber would improve combustion efficiency by extending propellant stay time. The linear relationships between pressure, characteristic length, and combustion efficiency provide predictive capability for igniter performance. For a given chamber geometry and propellant combination, the achievable efficiency can be estimated from the target operating pressure. The slopes of the correlations also quantify sensitivity to design changes. The scaling relationships can guide igniter optimization for specific test stand operations.

VI. Conclusion

An ultra-lean, modular, and cost effective augmented spark igniter was developed and validated for rocket engine test stand applications requiring extreme operational flexibility. The design employed interchangeable choked orifices to achieve independent control of mass ratio and igniter chamber pressure while sharing gaseous oxygen and methane propellant supplies with the main chamber. The approach eliminated dedicated igniter propellant systems. The elimination reduced facility complexity and cost while maintaining operational capability across a wide parameter testing range.

Three experimental campaigns systematically validated the igniter performance. The first demonstrated repeatability through ten consecutive successful atmospheric discharge tests. The second verified main chamber ignition capability by successfully igniting a fuel-rich main chamber across ten consecutive tests. The third characterized operational limits, achieving self-ignition from mass ratio 11.14 to 30.74 and igniter chamber pressure 627 to 2034 kPa. All design objectives were met, including ultra-lean operation exceeding MR 20 and igniter chamber pressures above 1379 kPa, as specified by MSFC requirements.

Combustion efficiency correlated strongly with igniter chamber pressure ($R^2 = 0.9371$), ranging from 30% at 627 kPa to 95% at 2034 kPa. The linear relationship arose from the propellant stay time effects quantified through the characteristic chamber length. Higher pressure increases gas density, extending propellant stay time for a fixed chamber geometry and enabling more complete combustion. The efficiency also correlates with normalized characteristic length ($R^2 = 0.9647$), with high pressure tests operating above the physical L' achieving the highest performance. These linear relationships provide predictive capability for igniter performance and guide optimization for specific pressure regimes.

The work establishes a practical igniter solution for RDRE and other advanced propulsion test programs requiring wide parametric exploration. The interchangeable orifice concept enables systematic coverage of mass ratio and pressure without hardware redesign. The propellant stay time framework explains observed performance trends and provides scaling relationships for future designs.

VII. Acknowledgments

The authors would like to thank NASA for financial support via grant 80NSSC22M0198 and Dillon Petty for supporting the work. We also thank masters student Murphy Mitchell for his work in conducting the cold flow testing of the laser-drilled orifices, and undergraduate students Evan Van Daniker, Evan Wagoner, Grant Poole, and Kyle Kibby for their assistance in the construction and operation of the igniter test stand.

Appendix

Test	P_{O_2} (psig)	P_{CH_4} (psig)	P_c (psig)	MR	$\dot{m}_{total}$ (lbm/s)	C^*_η
1	885.57	819.96	116.78	11.14	0.00499	46%
2	1214.56	821.72	91.34	15.25	0.00669	30%
3	1230.01	823.17	140.05	15.41	0.00676	44%
4	1220.16	822.64	141.02	15.30	0.00672	44%
5	1219.88	823.66	91.33	15.29	0.00672	30%
6	1220.02	822.09	128.06	15.33	0.00672	40%
7	1040.09	813.88	196.71	13.20	0.00579	66%
8	1201.28	497.55	243.43	25.12	0.00647	90%
9	1185.59	642.54	212.67	30.74	0.00633	87%
10	1216.83	1073.58	294.90	18.61	0.00664	95%

Table 3 Data for each successful test run in the third campaign, including test number, oxygen input pressure (P_{O_2}), methane input pressure (P_{CH_4}), hot gas pressure (P_c), mass ratio (MR), hot gas mass flow rate ($\dot{m}_{total}$), and characteristic velocity efficiency (C^*_η).

References

[1] Coward, H. F., and Jones, G. W., "Limits of Flammability of Gases and Vapors," , 1952. AD701575.

[2] Zabetakis, M. G., "Flammability Characteristics of Combustible Gases and Vapors," , 1965.

[3] Sutton, P. G., and Biblarz, O., *Rocket Propulsion Elements*, Wiley-Intersicience, New York, United States, 2001.

[4] Huzel, K. D., and Huang, H. D., "Design of Liquid Propellant Rocket Engines," , January 1967. 71N29405.

[5] Tinker, D. C., "Compact Augmented Spark Igniters For Liquid Rocket Engines," , 2021.

[6] Rudman, T. J., and Austad, K. L., "Evolution of Pratt and Whitney's Cryogenic Rocket Engine RL-10," *4th International Conference on Launcher Technology*, Liege, Belgium, 2002, pp. 1–2.

[7] Shynkarenko, O., Simone, D., Lee, J., and Bertoldi, A. E. M., "Experimental and Numerical Study of the Flammability Limits in a CH4/O2 Torch Ignition System," *Energies*, 2022.

[8] "J-2 ENGINE," *Saturn V News Reference*, 1968.

[9] Marshall, W. M., Osborne, R. J., and Greene, S. E., "Development of Augmented Spark Impinging Igniter System for Methane Engines," *53rd AIAA/SAE/ASEE Joint Propulsion Conference*, 2017.

[10] Teasley, T. W., Protz, C. S., Larkey, A. P., Williams, B. B., and Gradl, P. R., "A Review Towards the Design Optimization of High Performance Additively Manufactured Rotating Detonation Rocket Engine Injectors," *AIAA Propulsion and Energy Forum 2021*, 2021.

[11] Zlochower, I. A., and Green, G. M., "The limiting oxygen concentration and flammability limits of gases and gas mixtures," *Journal of Loss Prevention in the Process Industries*, 2009.

[12] Huang, L., Wang, Y., Pei, S., Cui, G., Zhang, L., Ren, S., Zhang, Z., and Wang, N., "Effect of elevated pressure on the explosion and flammability limits of methane-air mixtures," *Energy*, 2019.

[13] Huzel, K. D., and Huang, H. D., *Modern Engineering for Design of Liquid Propellant Rocket Engines*, Vol. 147, American Institude of Aeronautics and Astronautics, 1992.

[14] Goodwin, D. G., Moffat, H. K., Schoegl, I., Speth, R. L., and Weber, B. W., "Cantera: An Object-oriented Software Toolkit for Chemical Kinetics, Thermodynamics, and Transport Processes," `https://www.cantera.org`, 2025. https://doi.org/10.5281/zenodo.17620923, version 3.2.0.

[15] Smith, G. P., Golden, D. M., Frenklach, M., Moriarty, N. W., Eiteneer, B., Goldenberg, M., Bowman, C. T., Hanson, R. K., Song, S., Gardiner, W. C., Lissianski, V. V., and Qin, Z., "GRI-Mech 3.0," http://www.me.berkeley.edu/gri_mech/, 1999.